

See discussions, stats, and author profiles for this publication at: <https://www.researchgate.net/publication/263294419>

Water-Mediated Proton Conduction in a Robust Triazolyl Phosphonate Metal–Organic Framework with Hydrophilic Nanochannels

ARTICLE *in* CHEMISTRY · JUNE 2014

Impact Factor: 5.73 · DOI: 10.1002/chem.201402886 · Source: PubMed

CITATIONS

5

READS

56

11 AUTHORS, INCLUDING:



Salma Begum

University of Leipzig

3 PUBLICATIONS 11 CITATIONS

SEE PROFILE



Ferdinando Costantino

Università degli Studi di Perugia

71 PUBLICATIONS 786 CITATIONS

SEE PROFILE



Rustem Valiullin

University of Leipzig

137 PUBLICATIONS 1,646 CITATIONS

SEE PROFILE



Christian Chmelik

University of Leipzig

73 PUBLICATIONS 1,290 CITATIONS

SEE PROFILE

Porous Materials

Water-Mediated Proton Conduction in a Robust Triazolyl Phosphonate Metal–Organic Framework with Hydrophilic Nanochannels

Salma Begum,^[a] Zhaoyang Wang,^[a] Anna Donnadio,^[b] Ferdinando Costantino,^[b] Mario Casciola,^[b] Rustem Valiullin,^[c] Christian Chmelik,^[c] Marko Bertmer,^[c] Jörg Kärger,^[c] Jürgen Haase,^[c] and Harald Krautscheid^{*[a]}

Dedicated to Professor Joachim Sieler on the occasion of his 75th birthday

Abstract: The development of water-mediated proton-conducting materials operating above 100 °C remains challenging because the extended structures of existing materials usually deteriorate at high temperatures. A new triazolyl phosphonate metal–organic framework (MOF) [La₃L₄(H₂O)₆]Cl·xH₂O (**1**, L^{2−} = 4-(4H-1,2,4-triazol-4-yl)phenyl phosphonate) with highly hydrophilic 1D channels was synthesized hydrothermally. Compound **1** is an example of a phosphonate MOF with large regular pores with 1.9 nm in diameter. It forms a water-stable, porous structure that can be reversibly hydrated and dehydrated. The proton-conducting properties of **1** were investigated by impedance spectroscopy. Magic-angle spinning (MAS) and pulse field gradient (PFG) NMR spectroscopies confirm the dynamic nature of the incorporated water molecules. The diffusivities, determined by PFG NMR and IR microscopy, were found to be close to that of liquid water. This porous framework accomplishes the challenges of water stability and proton conduction even at 110 °C. The conductivity in **1** is proposed to occur by the vehicle mechanism.

The fast-growing diverse field of proton-conducting metal–organic frameworks (MOFs) is currently explored for promising applications as proton-exchange membranes, which is one of the key components in fuel-cell technology.^[1–3] Nafion and Nafion-like polymer membranes are efficient proton conductors,^[4,5] however the high costs and temperature limitations have driven a number of strategies towards the design of alternative materials, such as mesoporous silica,^[6] coordination


polymers (CPs),^[1,7] and porous organic solids.^[8] The first study of proton conduction in a 2D copper- and dithioxamide-based CP was reported in 1979 by Kanda et al.^[9] Kitagawa et al.^[10] extended this work by using derivatives of dithioxamides as organic linkers and reported the first systematic study on proton conduction in CPs. Compared with carboxylate, phosphonate-based MOFs are considerably scarce in the literature,^[11] most of the proton-conducting phosphonate MOFs have been reported by Shimizu et al.,^[12,13] with successful attempts to maintain also uncoordinated phosphonate functionalities protruding towards the pores as proton-conduction sites.^[14] From the perspective of synthesizing novel, proton-conducting, porous materials, phosphonate-based MOFs are considered good candidates owing to the acidity of the P–OH groups, to the high chemical and thermal stability and to the high versatility to crystallize in different structural architectures.^[15,16] The design of phosphonate MOFs with permanent porosity is still considered a challenge as the high number of P–O groups potentially coordinating to metal atoms and the effect of noncovalent interactions need to be combined for the achievement of the desired porous compounds (Figure 1).

Although a number of crystalline porous phosphonate MOFs has been prepared using low-valent cations,^[17,18] trivalent and tetravalent metal phosphonates are rarely crystalline^[15] and some of them possess interlayer porosity.^[19] By functionalization of phenyl phosphonate with a triazole ring as additional donor group, it was possible to grow single crystals of 3D porous phosphonate MOFs based on trivalent metal ions—contrary to the established trend of phosphonates that often precipitate as microcrystalline products. Availability of single-crystal structure data of robust proton-conducting materials could potentially fill the gap to establish a basis for the struc-

[a] S. Begum, Z. Wang, Prof. Dr. H. Krautscheid
Fakultät für Chemie und Mineralogie
Universität Leipzig
Johannisallee 29, 04103 Leipzig (Germany)
E-mail: krautscheid@rz.uni-leipzig.de

[b] Dr. A. Donnadio, Prof. Dr. F. Costantino, Prof. Dr. M. Casciola
Department of Chemistry
University of Perugia
Via Elce di Sotto n.8, Perugia (Italy)

[c] Dr. R. Valiullin, Dr. C. Chmelik, Dr. M. Bertmer, Prof. Dr. J. Kärger,
Prof. Dr. J. Haase
Fakultät für Physik und Geowissenschaften
Universität Leipzig
Linnéstrasse 5, 04103 Leipzig (Germany)

 Supporting information for this article, including experimental details for ligand and MOF syntheses, characterization by X-ray diffraction and TG/DTA-MS, ¹H and ³¹P solid-state NMR, impedance spectroscopy, IR microscopy, and PFG NMR data, is available on the WWW under <http://dx.doi.org/10.1002/chem.201402886>.

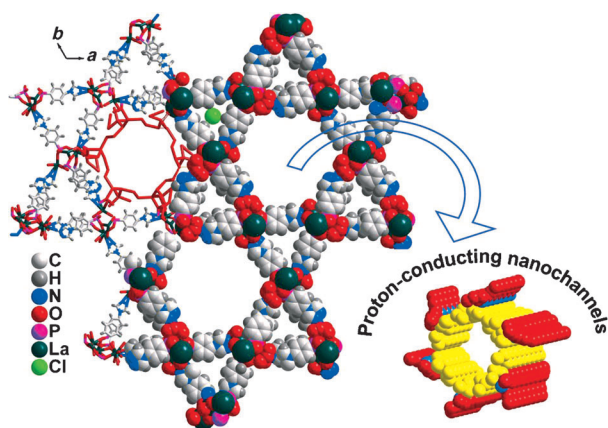


Figure 1. Fragment of the crystal structure of **1**,^[21] view along [001]. The arrow directs to the enlarged 1D channels (1.9 nm in diameter) filled with noncoordinated (yellow) and coordinated (red) water molecules; phosphate free oxygen atoms are shown in light blue.

ture–activity relationship that has remained a challenge in the field of noncrystalline electrolytes.^[2, 5, 20]

Herein, we report on the triazolyl phosphonate based La^{3+} MOF $[\text{La}_3\text{L}_4(\text{H}_2\text{O})_6]\text{Cl}\cdot x\text{H}_2\text{O}$ (**1**, $\text{L}^{2-} = 4\text{-(4H-1,2,4-triazol-4-yl)-phenyl phosphonate}$) with wide hydrophilic nanochannels. These channels with a unique structural arrangement of water molecules make **1** interesting for investigation of proton-conducting properties.

Compound **1** crystallizes in the trigonal space group $P\bar{3}$ (no. 147) with four crystallographically independent linker anions L^{2-} and three La^{3+} ions in the asymmetric unit.^[21] A charge-balancing chloride ion is detected in the elemental analysis, but could only partly be localized in the structure refinement. With La–O bond lengths from 230 to 283 pm and La–N bond lengths from 270 to 278 pm the La^{3+} ions have coordination number nine. Six of the 27 coordination sites for the three La^{3+} ions are occupied by water molecules, the remaining ones are occupied by four nitrogen atoms of three triazole rings, five terminal and six bridging oxygen atoms of the phosphonate groups. The μ_4 -, μ_5 -, and μ_6 -bridging triazolyl phenylphosphonate linkers connect the La^{3+} ions into a 3D network; the projection along [001] resembles a Kagomé-type net (Figure 1).

The coordinated water molecules and noncoordinating phosphonate-oxygen atoms O3 form 1D chains through hydrogen bonds ($\text{O}\cdots\text{O}$ 264–316 pm), which extend along the crystallographic c direction. Six such chains combine to highly hydrophilic hexagonal channels that retain physisorbed water molecules inside the pores. These channels are arranged like a hexagonal packing of rods and show a visible open diameter of 1.9 nm (Figure 1). Based on crystal-structure data a solvent-accessible pore volume of 38% is calculated.^[22] Regular pores with a diameter of 1.8 nm in the isoreticularly constructed bis-piperidine diphosphonate MOF by Wright et al. are the largest among the phosphonate frameworks reported to date.^[18]

Framework hydrostability is a special characteristic required for proton-conducting hydrous materials in humid environments. The effect of dehydration and complete rehydration of

1 was scrutinized initially by evacuating at 1×10^{-5} mbar and 40°C for 24 h to remove the noncoordinating water molecules while the evacuated samples were rehydrated by exposing them to water. Keeping the samples for five days in refluxing water did not change the diffraction patterns. The PXRD patterns (Figure SI-2 in the Supporting Information) and TGA graphs (Figure SI-3 in the Supporting Information) indicate that the material is insoluble and stable in water. The TGA curve of air-dried **1** shows a mass loss of 17 wt% in three steps in the temperature range up to 450°C . The first two steps are attributed to the loss of noncoordinated and coordinated water molecules at about 90°C and at $180\text{--}210^\circ\text{C}$, respectively. The weight loss varies significantly with the drying conditions, indicating that the capacity of **1** to accommodate water molecules in nanochannels is strongly influenced by its surrounding temperature and humidity. The first weight loss (3.6%) of the evacuated sample corresponds to three H_2O molecules per formula unit (calcd 3.7%).

Furthermore, the dynamic nature of physisorbed water molecules is confirmed by the comparison of solid-state ^1H NMR spectra of evacuated and hydrated samples of **1** (Figure SI-4a in the Supporting Information). In the hydrated sample with a chemical shift of 4.2 ppm (close to that of free water), the resonance of the coordinated water molecules cannot be seen as separate signal because of the fast exchange with the mobile water molecules. In the evacuated sample this resonance appears at 6.8 ppm. The ^1H NMR signal intensity of a hydrated sample corresponds to 84 protons referring to 42 water molecules (78% of the overall intensity) in comparison to 24 protons (22%) belonging to the organic linkers (Figure SI-4a in the Supporting Information). The comparison of ^1H magic-angle spinning (MAS) and ^1H double quantum (DQ) filtered NMR spectra (Figure SI-4b in the Supporting Information) allows to differentiate the mobile species that contribute to the proton transport from those bound to the MOF. The absence of a water-proton signal at 4.2 ppm in the DQ spectra indicates that the dipole–dipole coupling among these protons is weak and rapid isotropic molecular tumbling averages the magnetic dipolar coupling to zero. Variable-temperature studies were performed in the temperature range from -4 to 65°C . The line narrowing of the resonance at 4.2 ppm with increasing temperatures agrees well with dynamic exchange with an activation energy of 0.07 eV (Figure SI-5 in the Supporting Information).

The ionic conductivity (σ) of **1** was investigated by complex impedance ($Z^* = Z' - iZ''$) measurements carried out on pellets as a function of relative humidity (RH) at temperatures up to 110°C . The conductivity of the pellets was calculated from the analysis of Nyquist plots (Z'' vs. Z') as described in Supporting Information. The dependence of σ on RH at a constant temperature is shown in Figure 2a: In particular, at 110°C and in the RH range 20–98%, σ increases with RH by three orders of magnitude reaching $1.7\times 10^{-4}\text{ Scm}^{-1}$. To the best of our knowledge, **1** is the first example of a hydrated MOF that allows gradual increase in ionic conductance by raising the temperature up to 110°C . In contrast, conductivity studies on most MOFs have not been reported at elevated temperatures.^[1] At

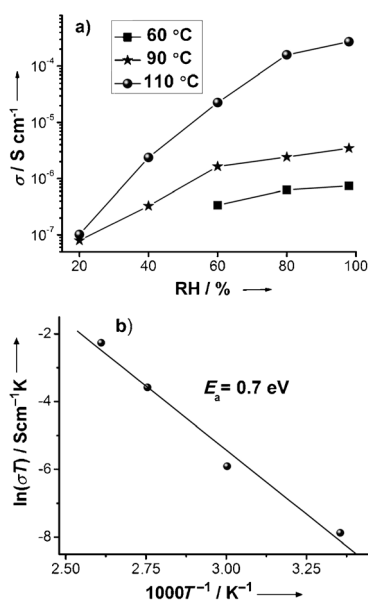


Figure 2. Proton-conductivity data for **1**. a) As a function of RH at different temperatures and b) Arrhenius plot of the activation energy at 98% RH for the temperature range 25–110 °C.

a constant RH of 98%, the activation energy for conduction ($E_a = 0.7$ eV), calculated from the Arrhenius plot (Figure 2b), is significantly higher than those reported for proton-conducting phosphonate MOFs, such as PCMOF-3^[12] ($E_a = 0.17$ eV), PCMOF-5^[14] ($E_a = 0.16$ eV), or ZrCyclo^[23] ($E_a = 0.23$ eV), but lower than recently reported values for two tetracarboxylate-based lanthanide MOFs ($E_a = 0.9$ eV).^[24]

To investigate the nature of the charge carriers in **1**, impedance measurements were performed at 25 °C under a flow of humidified N₂ and H₂ (see the Supporting Information for details): In the presence of hydrogen the Pt electrodes are reversible towards the redox process involving protons, whereas they are ideally blocked in the presence of nitrogen. As expected, the Nyquist plot collected under N₂ (Figure 3a) shows a large capacitive tail at low frequency; this indicates that the electrodes are substantially blocked. Under H₂, the low-frequency tail shrinks by a factor of about 70 (Figure 3b), giving rise to a small arc followed, at low frequencies, by a straight

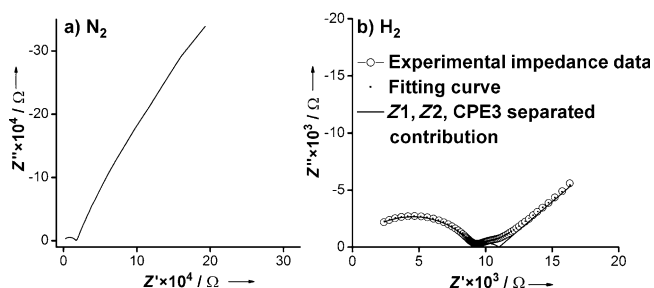


Figure 3. Nyquist plots for **1** at 25 °C a) under humidified N₂ at 100% RH and b) under humidified H₂ at 100% RH. Z1, Z2, and CPE3 are the elements of the equivalent circuit (Figure SI-7 in the Supporting Information) used to model the frequency response of the pellet.

line inclined by 45° with respect to the Z' axis; this is typical of the Warburg impedance. Accordingly, Figure 3b shows that the frequency response of the pellet–electrode assembly can be accurately modelled by an equivalent circuit (Figure SI-7 in the Supporting Information) where the electrode–electrolyte interface is represented by a Warburg element connected with a parallel combination of a resistance and a constant phase element, which accounts for the charge-transfer process. The strong reduction of the low-frequency tail indicates the presence of mobile protonic species (H₃O⁺, OH[−]), which take part in the electrode reactions and concentration of these species may be enhanced either by deprotonation of water molecules coordinated to La³⁺ or by protonation of triazole groups and/or free phosphonate oxygen atoms. According to Archer,^[25] the appearance of the Warburg impedance when N₂ is replaced by H₂ is consistent with the presence of two charge carriers, one of which is blocked at the electrodes. These findings and presence of partially disordered chloride ions in the crystallographic data suggest that a fraction of the charge-balancing chloride ions might be located in the MOF channels and partially contribute to the ionic conduction together with the protonic species. When the impedance measurements are carried out with an applied DC voltage of 0.1 and 0.2 V (Figure SI-9 and 10 in the Supporting Information), the arc representing the frequency response of the pellet remains substantially unchanged, whereas, with increasing the DC voltage, a progressive growth of the impedance of the electrode–electrolyte interface is observed; this can be ascribed to electrode-polarization phenomena.

To get insight into the interaction energy of water molecules in 1D confinement, diffusion studies were carried out by IR microscopy^[26] and pulsed field gradient (PFG) NMR.^[27] To estimate the degree of pore filling at each chosen pressure and temperature, equilibrium adsorption isotherms were recorded in the temperature range of 25–110 °C (Figure 4a). Due to the pressure limitations of the instrumental setup only at 25 °C and 40 °C full pore filling is reached, as evidenced by the sharp condensation steps in the isotherms occurring at 7 and 18 mbar, respectively. No change in the adsorption capacity and uptake rates was evidenced during a series of experiments with the same crystal; this testifies again the excellent stability of **1** in a humid environment and at temperatures up to 110 °C.

To cover the full range of pore fillings the loading dependence of the transport diffusivity was investigated at 40 °C (Figure 4b). Two regions can be distinguished. At intermediate-to-high pore fillings, the transport diffusivity is roughly constant at about $D_T = 1.5 \times 10^{-9}$ m² s^{−1}. At low-to-intermediate loadings, we find a strongly increasing transport rate. This is typical for systems with strong interaction sites at the pore walls (type-III concentration dependence of diffusivities^[26b,28] observed, e.g., with water and ammonia in zeolite NaX^[29] and ammonia in MFI-type zeolites).^[30] The number of free sites decreases with increasing coverage, while, in turn, the mobility of the guest water molecules increases. The existence of strong interaction sites is supported by the particularly high activation energy for diffusion at zero loading of about $E_a = 0.48$ eV, which was esti-

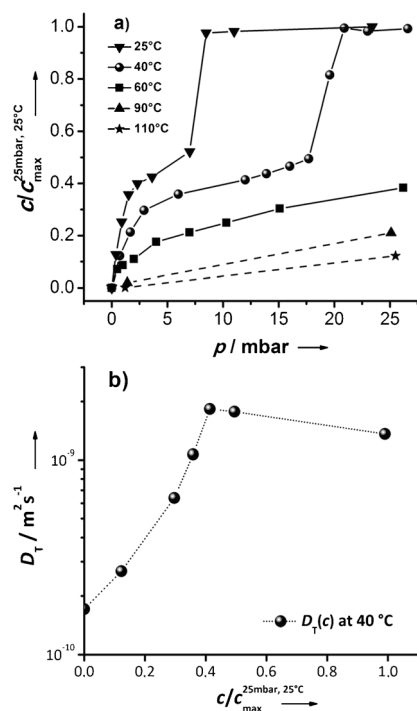


Figure 4. a) Adsorption isotherms of water in **1** at different temperatures measured by IR microscopy. All curves are normalized to the maximum loading reached for water vapor pressure at 25 °C to indicate the degree of pore filling. b) Diffusivity of water in **1** as obtained from IR microscopy measurements; dependence of the transport diffusivity D_t on the degree of pore filling at 40 °C.

mated from the zero loading diffusivities between 25 and 110 °C by assuming Arrhenius law behavior ($D = D_\infty \times \exp(-E_a/RT)$), Figure SI-11 in the Supporting Information). Even though this high activation energy leads to an increase of the zero-loading diffusivities by about two orders of magnitude, this trend might be much less pronounced for higher pore filling.

To confirm the long-range mobility of water molecules along the 1D channels in **1** ^1H PFG NMR^[27] self-diffusion studies were carried out. The diffusion coefficients of $1.2 \times 10^{-9} \text{ m}^2 \text{ s}^{-1}$ determined by PFG NMR and $1.5 \times 10^{-9} \text{ m}^2 \text{ s}^{-1}$ determined by IR microscopy^[26] are found to be close to that of liquid water with $2.2 \times 10^{-9} \text{ m}^2 \text{ s}^{-1}$.^[31] This indicates liquidlike behavior of the channel water molecules. The obtained diffusivities D_0 ($1.2 \times 10^{-9} \text{ m}^2 \text{ s}^{-1}$) have shown almost no dependence on the diffusion time up to 200 ms, revealing structural integrity of the channels on the length scale of 20 μm . The activation energy for diffusion is determined as $E_a = 0.062 \text{ eV}$ (Figure SI-12b in the Supporting Information, temperature range 25–110 °C). The significant difference between activation energies received through impedance spectroscopy (IS) ($E_a = 0.7 \text{ eV}$) and PFG-NMR originates in the different length scales on which the transport properties are probed, macroscopic for IS and microscopic for PFG NMR.

In summary, **1** is a 3D triazolyl-phosphonate-based La^{3+} MOF with large hydrophilic channels (1.9 nm) containing water molecules as proton-conducting medium. This porous framework with a specific chemical environment (coordinated water

molecules, noncoordinating phosphonate oxygen atoms, triazole groups, and plenty of uncoordinated water molecules) accomplishes the challenges of water stability and proton conduction even at 110 °C. The proton conductivity increases significantly with increasing temperature and relative humidity by facilitating charge formation and maintaining high charge density, respectively. MAS and PFG NMR confirm the dynamic nature of the water molecules and that the water molecules are free to diffuse for long distances of at least 20 μm along 1D channels in the framework of **1**.

Acknowledgements

We thank Dr. M. Kischel for assistance with TG-MS, Dr. H. J. Stärk (UFZ Leipzig) for performing the chloride analysis, M. Lange and Dr. J. Möllmer (INC Leipzig) for adsorption measurements and helpful discussions and Experimental Physics Institutes (Universität Leipzig) for support with the Avance 750 MHz NMR spectrometer. Financial support from Deutsche Forschungsgemeinschaft (SPP 1362—Poröse metallorganische Gerüstverbindungen, KR 1675/7-2), Universität Leipzig (PbF-1) and the graduate school BuildMoNa is gratefully acknowledged. S. Begum acknowledges financial support from Higher Education Commission Pakistan and a fellowship by DAAD.

Keywords: diffusion studies • impedance spectroscopy • metal–organic frameworks • microporous materials • proton conduction

- [1] M. Yoon, K. Suh, S. Natarajan, K. Kim, *Angew. Chem.* **2013**, *125*, 2752–2764; *Angew. Chem. Int. Ed.* **2013**, *52*, 2688–2700.
- [2] M. Schuster, T. Rager, A. Noda, K. D. Kreuer, J. Maier, *Fuel Cells* **2005**, *5*, 355–365.
- [3] S. Peighambarpour, S. Rowshanzamir, M. Amjadi, *Int. J. Hydrogen Energy* **2010**, *35*, 9349–9384.
- [4] M. A. Hickner, B. S. Pivovar, *Fuel Cells* **2005**, *5*, 213–229.
- [5] K. A. Mauritz, R. B. Moore, *Chem. Rev.* **2004**, *104*, 4535–4585.
- [6] S. Suzuki, Y. Nozaki, T. Okumura, M. Miyayama, *J. Ceram. Soc. Jpn.* **2006**, *114*, 303–307.
- [7] J. A. Hurd, R. Vaidhyanathan, V. Thangadurai, C. I. Ratcliffe, I. L. Moudrakovski, G. K. H. Shimizu, *Nat. Chem.* **2009**, *1*, 705–710.
- [8] J. W. Lee, S. Samal, N. Selvapalam, H.-J. Kim, K. Kim, *Acc. Chem. Res.* **2003**, *36*, 621–630.
- [9] a) S. Kanda, K. Yamashita, K. Ohkawa, *Bull. Chem. Soc. Jpn.* **1979**, *52*, 3296–3301; b) S. Kanda, Y. Fumio, *Bull. Chem. Soc. Jpn.* **1996**, *69*, 477–483.
- [10] a) Y. Nagao, R. Ikeda, S. Kanda, Y. Kubozono, H. Kitagawa, *Mol. Cryst. Liq. Cryst.* **2002**, *379*, 89–94; b) H. Kitagawa, Y. Nagao, M. Fujishima, R. Ikeda, S. Kanda, *Inorg. Chem. Commun.* **2003**, *6*, 346–348.
- [11] R. M. P. Colodrero, P. Olivera-Pastor, E. R. Losilla, D. Hernández-Alonso, M. A. G. Aranda, L. Leon-Reina, J. Rius, K. D. Demadis, B. Moreau, D. Villamin, *Inorg. Chem.* **2012**, *51*, 7689–7698.
- [12] J. M. Taylor, R. K. Mah, I. L. Moudrakovski, C. I. Ratcliffe, R. Vaidhyanathan, G. K. H. Shimizu, *J. Am. Chem. Soc.* **2010**, *132*, 14055–14057.
- [13] S. Kim, K. W. Dawson, B. S. Gelfand, J. M. Taylor, G. K. H. Shimizu, *J. Am. Chem. Soc.* **2013**, *135*, 963–966.
- [14] J. M. Taylor, K. W. Dawson, G. K. H. Shimizu, *J. Am. Chem. Soc.* **2013**, *135*, 1193–1196.
- [15] K. J. Gagnon, H. P. Perry, A. Clearfield, *Chem. Rev.* **2012**, *112*, 1034–1054.
- [16] S. Natarajan, P. Mahata, *Curr. Opin. Solid State Mater. Sci.* **2009**, *13*, 46–53.
- [17] a) J. A. Groves, S. R. Miller, S. J. Warrender, C. Mellot-Draznieks, P. Lightfoot, P. A. Wright, *Chem. Commun.* **2006**, 3305; b) M. Taddei, F. Costanti-

- no, A. Ienco, A. Comotti, P. V. Dau, S. M. Cohen, *Chem. Commun.* **2013**, 49, 1315.
- [18] M. T. Wharmby, J. P. S. Mowat, S. P. Thompson, P. A. Wright, *J. Am. Chem. Soc.* **2011**, 133, 1266–1269.
- [19] a) J. A. Groves, P. A. Wright, P. Lightfoot, *Inorg. Chem.* **2005**, 44, 1736–1739; b) A. Clearfield, *Chem. Mater.* **1998**, 10, 2801–2810; c) G. Alberti, U. Costantino, F. Marmottini, R. Vivani, P. Zappelli, *Angew. Chem.* **1993**, 105, 1396; *Angew. Chem. Int. Ed. Engl.* **1993**, 32, 1357; d) G. Alberti, R. Vivani, F. Marmottini, S. Murcia Mascarós, *Angew. Chem.* **1994**, 106, 1655; *Angew. Chem. Int. Ed. Engl.* **1994**, 33, 1594.
- [20] S. Bose, T. Kuila, T. X. H. Nguyen, N. H. Kim, K.-t. Lau, J. H. Lee, *Prog. Polym. Sci.* **2011**, 36, 813–843.
- [21] Crystal data: **1** ($C_{32}H_{35}N_{12}La_3O_{18}P_4$): Stoe IPDS-2T Diffractometer, $M_r = 1416.2 \text{ g mol}^{-1}$, crystal size $0.8 \times 0.1 \times 0.1 \text{ mm}^3$, trigonal, space group $P\bar{3}$ (no. 147), $a = 3057.3(4)$, $c = 1352.1(3)$, $Z = 6$, $T = 180(2) \text{ K}$, $V = 10944(3) \times 10^6 \text{ pm}^3$, $\rho_{\text{calc}} = 1.323 \text{ g cm}^{-3}$, $\mu = 1.904 \text{ mm}^{-1}$, $\lambda = 71.073 \text{ pm}$ ($\text{Mo K}\alpha$), $T_{\text{min}} = 0.72$, $T_{\text{max}} = 0.89$, 24423 measured, 13678 independent reflections, $R_{\text{int}} = 0.056$, 8183 with $I > 2\sigma(I)$, 580 parameters, two phosphonate ligands and coordinating water molecules disordered, H atoms of phosphonate ligands in idealized positions, $R1$ (observed reflections) = 0.045, $wR2$ (all data) = 0.101, max/min residual-electron-density peaks $1.89 / -1.28 \text{ e}^{-}/10^6 \text{ pm}^3$. CCDC 934648 contains the supplementary crystallographic data for this paper. These data can be obtained free of charge from The Cambridge Crystallographic Data Centre via www.ccdc.cam.ac.uk/data_request/cif
- [22] A. L. Spek, *J. Appl. Crystallogr.* **2003**, 36, 7–13.
- [23] F. Costantino, A. Donnadio, M. Casciola, *Inorg. Chem.* **2012**, 51, 6992–7000.
- [24] M. Zhu, Z.-M. Hao, X.-Z. Song, X. Meng, S.-N. Zhao, S.-Y. Song, H.-J. Zhang, *Chem. Commun.* **2014**, 50, 1912.
- [25] H. R. Thirsk, W. I. Archer, *Electrochemistry: A Review of Recent Literature*, Chemical Society, London, **1980**, pp. 165–173.
- [26] a) C. Chmelik, J. Kärger, *Chem. Soc. Rev.* **2010**, 39, 4864; b) J. Kärger, D. M. Ruthven, D. N. Theodorou, *Diffusion in Nanoporous Materials*, Wiley-VCH, Weinheim, Germany, **2012**; c) J. Kärger, T. Binder, C. Chmelik, F. Hibbe, H. Krautscheid, R. Krishna, J. Weitkamp, *Nat. Mater.* **2014**, 13, 333–343.
- [27] R. Valiullin, J. Kärger, K. Cho, M. Choi, R. Ryoo, *Microporous Mesoporous Mater.* **2011**, 142, 236–244.
- [28] a) F. J. Keil, R. Krishna, M. O. Coppens, *Rev. Chem. Eng.* **2000**, 16, 71–197; b) J. Kärger, H. Pfeifer, *Zeolites* **1987**, 7, 90–107.
- [29] a) J. Kärger, *Z. Phys. Chem. (Leipzig)* **1971**, 248, 27–41; b) C. Forste, A. Germanus, J. Kärger, G. Möbius, M. Bülow, S. P. Zdanov, N. N. Feoktistova, *Isotopenpraxis* **1989**, 25, 48–52; c) P. Demontis, H. Jobic, M. A. Gonzalez, G. B. Suffritti, *J. Phys. Chem. C* **2009**, 113, 12373–12379.
- [30] H. Jobic, H. Ernst, W. Heink, J. Kärger, A. Tuel, M. Bee, *Microporous Mesoporous Mater.* **1998**, 26, 67–75; b) O. Geier, S. Vasenkov, D. Freude, J. Kärger, *J. Catal.* **2003**, 213, 321–323.
- [31] M. Holz, S. R. Heil, A. Sacco, *Phys. Chem. Chem. Phys.* **2000**, 2, 4740–4742.

Received: April 1, 2014
Published online on June 17, 2014